PEGylated bottom-up synthesized graphene nanoribbons loaded with camptothecin as potential drug carriers

H. Hou [a], L. Cardo [a], J.P. Merino [a,b], F. Xu [c], C. Wetzl [a,b], B. Arnaiz [a], X. Luan [c], Y. Mai [c,***], A. Criado [d,a,*], M. Prato [a,e,f,**]

[a] Center for Cooperative Research in Biomaterials (CIC BiomaGUNE), Basque Research and Technology Alliance (BRTA), Paseo de Miramon 194, Donostia-San Sebastián 20014, Spain
[b] University of the Basque Country UPV-EHU, Donostia-San Sebastián 20018, Spain
[c] School of Chemistry and Chemical Engineering, Frontiers Science Center for Transformative Molecules, Shanghai Key Laboratory of Electrical Insulation and Thermal Ageing, Shanghai Jiao Tong University, 800 Dongchuan Road, Shanghai 200240, China
[d] Universidade da Coruña, CICA – Centro Interdisciplinar de Química e Bioloxía, Rúa As Carballeiras, 15071 A Coruña, Spain
[e] Department OfChemical and Pharmaceutical Sciences, University of Trieste, Via L. Giorgieri 1, 3412 7 Trieste, Italy
[f] Ikerbasque, Basque Foundation for Science, 48013 Bilbao, Spain

A B S T R A C T

This work discusses the potential use of bottom-up synthesized graphene nanoribbons (GNRs) as nano-carriers for drug delivery systems (DDSs). GNRs have a high loading capacity for anticancer drugs due to their high specific surface area and non-covalent adsorption with hydrophobic anticancer drug molecules. Herein, we synthesized GNRs using a bottom-up approach, modified with PEG2000 (GNR-PEG) and PEG2000 carrying folic acid chains (GNR-PEG-FA), and then loaded with camptothecin (CPT). The targeting ability mediated by folic acid of the GNR derivative was evaluated using cellular assays, and the cytotoxicity of GNR systems loaded with CPT was assessed by *in vitro* studies. They suggest that the functionalization of GNR derivatives with folic acid significantly affects their interaction with cells expressing different levels of folic acid receptors. The authors also explore the possibility to employ GNRs in photothermal therapy (PTT). GNR-PEG and GNR-PEG-FA display minor or no toxicity in standard cell cultures, but they show remarkable thermal response upon NIR irradiation, causing complete loss of cell viability within a few hours of treatment. This work highlights the potential of GNRs as DDSs and emphasizes the importance of further research on their biocompatibility and as a platform for PTT.

1. Introduction

Cancer is an abnormal growth of cells in the body that led to nearly 10 million human deaths in 2022. Globally, cancer is the second leading cause of death (about 1 in 6 deaths) [1]. And it is predicted that 13 million people will die of cancer in 2030 [2]. Nowadays, cancer is often treated in clinic with some combination of surgery, radiation therapy, and chemotherapy [3–5]. Among them, chemotherapy is a dominant category of cancer treatment, which includes one or more anti-cancer drugs. Furthermore, the pharmaceutical industry has been spending significant effort to improve the target specificity of anti-cancer drugs and reduce the undesired effects of systemic treatment [6]. However, various drugs used in clinic treatment are hydrophobic molecules (many of them are aromatic), have poor physiological stability, and present non-specific targeting/low drug efficacy, which lead to the intrinsic limitations for the applications of anti-cancer [7,8]. Therefore, alternative strategies able to achieve the above goals are highly desirable.

Graphene-based materials (GBMs) [9–11] have aroused great interest as potential drug delivery systems (DDSs) with high loading capacity for anticancer drugs due to extremely high specific surface area, non-covalent adsorption with hydrophobic anti-cancer drug molecules [10,12–14]. Different GBMs, such as graphene oxide (GO), reduced GO, hydrated GO, and graphene quantum dots, were used for the preparation of therapeutic systems [15].

* Corresponding author.
** Corresponding author.
*** Corresponding author.
E-mail addresses: mai@sjtu.edu.cn (Y. Mai), a.criado@udc.es (A. Criado), mprato@cicbiomagune.es (M. Prato).

One member of the GBM family that is gaining attention is called graphene nanoribbon (GNR). GNR can be synthesized using various methods such as the top-down [16–18] and bottom-up strategies [19, 20]. Among the top-down methods, oxidized GNRs (O-GNRs) obtained by oxidizing multi-walled carbon nanotubes (MWCNTs) with the longitudinal unzipping method are a popular choice for DDSs. For example, a PEG-DSPE-coated O-GNR system loaded with lucanthone, enhance drug uptake by the glioblastoma cell line U251 [21]. O-GNRs can also be used as delivery platforms able to improve the cellular penetration of highly hydrophobic ceramides [22]. However, there are not much research is available on using GNRs that are created through a bottom-up approach for DDSs. The precise control of GNRs' structures enables fine-tuning of dimensions and properties [23], resulting in optimized DDS features such as enhanced drug loading capacity and controlled release kinetics [24]. The ability to modify GNRs' structure facilitates efficient bioactive through pi-pi interactions [25], while precise modification of the graphene structure can potentially accommodate structurally relevant substituents [26]. In addition, their inherent stability can ensure sustained drug release and minimizes degradation [27]. Overall, these distinctive advantages position bottom-up synthesized GNRs as a promising and reliable platform for the future development of effective DDSs [28].

In the development of DDSs, folic acid (FA) is a well-known cancer-targeting molecule due to its high affinity for tumor cells, in which FA receptors are overexpressed. For example, FA combined with GBMs is able to induce a selective internalization of the material [29–31].

Although GNRs have shown great potential for biomedical applications, their biocompatibility and cytotoxicity remain an important concern [32]. Recent studies have suggested that the shape, and surface functionalization of GNRs play a crucial role in determining their toxicity [33,34]. While some studies have shown that GNRs exhibited good biocompatibility with human cell lines [21,35,36], others have revealed toxic effects, including cytotoxicity and genotoxicity [37,38]. Overall, more research is needed to fully understand the biocompatibility and cytotoxicity of GNRs, and to develop safe and effective applications for these materials in biomedicine.

Herein, we report bottom-up synthesized GNRs that were modified with PEG_{2000} (GNR-PEG) and PEG_{2000}-FA (GNR-PEG-FA), as nanocarriers for DDSs. Previous works have demonstrated that aromatic molecules can be loaded on GNRs via the pi-pi interaction [25]. Thus, the cytotoxic quinoline alkaloid camptothecin (CPT), which is a topoisomerase-I inhibitor that causes DNA damage and apoptosis [39, 40], was selected as an aromatic drug model. Then the targeting ability mediated by FA of the GNRs derivatives was evaluated using cellular assays. Subsequently, the cytotoxicity of GNR systems loaded with CTP (CPT@GNR-PEG and CPT@GNR-PEG-FA) was assessed by *in vitro* studies. Finally, since GBMs were previously reported to produce heating upon light irradiation, we explore the possibility of employing our material in photothermal therapy (PTT).

2. Experimental section

2.1. Synthesis of graphene nanoribbon (GNR)

The synthesis of GNR is according to the previous report [41].

2.2. Functionalization of GNR with FA−PEG or PEG

GNR (50 mg) was added to THF (60 mL) and sonicated for 4 h. Then EDC and NHS were added into the GNR dispersion and sonicated for 3 h. Finally, NH_2-PEG_{2000} or NH_2-PEG_{2000}-FA was put into the solution and stirred for 3 days at room temperature. Afterward, the mixture was dialyzed with a membrane of 10 kDa molecular weight cut-off against pure water by renewing the external water for more than 20 times over for 3 days to remove most of the unreacted FA−PEG or PEG.

2.3. CPT loading on GNR-FA−PEG and GNR-PEG

A CPT solution (5 mg, 14.3 mM) in DMSO (1 mL) was dropwise added to deionized water (10 mL) dispersions of GNR-FA−PEG or GNR-PEG. The resulting mixture was sonicated for 15 min and then stirred for 24 h at room temperature in dark. The non-bonded CPT was separated by filtration (filter from Omnipore Membrane, PTFE, filter type 0.45 μm) and washed three times with a mixture of water and MeOH (1:1/v:v, 10 mL), and deionized water (10 mL). Then the resulting materials were dispersed in deionized water (10 mL).

The capability of GNR-PEG-FA or GNR-PEG to carry CPT was evaluated in terms of LC% and LE% (details in supplementary data).

2.4. Cell viability assays

96 well-plates were seeded overnight with a defined number of cells (4000 of A549 and 5000 of MCF-7 per well in respective 100 μL of media). Cells were treated with triplicates of at least six different concentrations of each compound (GNR-PEG, GNR-PEG-FA, CTP@GNR-PEG, CTP@GNR-PEG-FA in respective media), typically from 0.05 up to 50 μM (referred to the concentration of CPT) and left in incubator (37 °C, 5% CO_2, 95% air). After the selected incubation time (24, 48, and 72 h were tested) cells were washed with PBS (4x) and treated with 100 mL of 3-(4,5-dimethylthiazolyl-2)-2, 5-diphenyltetrazolium bromide (MTT) in medium (final concentration 0.5 mg/mL) for 3 h. Medium was carefully removed from each well, the purple crystals of formazan dissolved in 200 μL DMSO and absorbance at 550 nm was measured using a microplate reader (GENios Pro, Tecan). Cell viability curves and statistic data (using two-way ANOVA) were generated with GraphPad 9.1 employing measurements from at least two independent repeats of triplicated experiments. A control experiment with material only (no cells) was performed in the same conditions to ensure that the eventual precipitated material was not affecting the colorimetric measurement.

2.5. Cell microscopy studies

24 well plates suitable for confocal microscopy (Cellvis, #1.5 high-performance cover glass) were seeded overnight with A549 (20,000 cells in 500 mL RPMI) or MCF-7 (30,000 in 500 mL DMEM). Both cell lines were treated with GNR or GNR-FA for 24 h (5, 10, and 20 mg/mL concentrations were tested, at 37 °C, 5% CO_2, 95% air) followed by washing with PBS (4x). Cells were left in medium for live cell imaging or treated with formalin followed by washing with PBS (3x) for fixed cell studies. All images were collected with an LSM 510 META laser scanning microscope (Zeiss) using a 20x or 40x air objective and processed with ImageJ.

2.6. In vitro photothermal assay

A549 (6000 cells in 100 mL RPMI, upon overnight seeding in black wall 96 well plates) were treated with 100 μg/mL of compound (GNR, GNR@CPT, or CPT, concentrations referring to GNR materials) for 10 h. Cells were exposed to NIR light using a fiber-coupled 808 nm diode laser (Lumics, LU808T040, power, 1.0 W; laser spot diameter, 6 mm) and the heat produced was monitored with a thermal camera (FLIR A35). All conditions (concentration of GNR material and power of irradiation) were optimized to increase the temperature of the sample to 41–42 °C during NIR irradiation, in a short time (typically 1 min). Each sample was irradiated for 6 min, noticing that temperature raised from rt to 41 °C during the first minute. In a second set of experiments, a second and a third irradiation were repeated after 2 h and 4 h, respectively. At the end of the NIR treatment cell viability was tested by MTT assay after 1 h from the last irradiation. Between treatments, cells were kept in incubator (37 °C, 5% CO_2, 95% air). Each time, an equal experiment was prepared in parallel, but the samples were kept in incubator, with the following MTT assay, to compare the effect of irradiation vs no

irradiation. Having 1, 2, or 3 NIR irradiation treatments did not produce any difference compared to the results shown in Fig. 4 (data not shown). Cell viability data were generated with GraphPad 9.1 employing measurements from at least three independent repeats of duplicate experiments.

3. Results and discussion

The GNR-PEG with an armchair edge structure was synthesized according to a reported protocol [41,42]. In summary, the GNR backbone was synthesized by Yamamoto polymerization of a dichloro-substituted oligophenylene monomer decorated with $–C_{10}H_{20}COOCH_3$ chains, followed by cyclodehydrogenation of the resultant polyphenylene and the hydrolysis of the ester groups to provide GNR-COOH. Then, GNR-COOH functional groups were functionalized with NH_2-PEG_{2000} or NH_2-PEG_{2000}-FA by EDC/NHS activation to afford the amide-linked functional nano-carriers GNR-PEG and GNR-PEG-FA, respectively (Scheme 1). It should be emphasized that the incorporation of PEGylated chains is crucial, as they enable remarkable solubility in both typical organic solvents and aqueous solutions [26,41]. This characteristic is absent in non-functionalized or functionalized GNRs that possess shorter alkyl chains.

The amidation of GNR-COOH was successfully confirmed by thermogravimetric analysis (TGA) and Fourier-transform infrared spectroscopy (FTIR). The FTIR characterization indicates the successful PEGylation of GNR-PEG and GNR-PEG-FA by the amide bond (Fig. S1). Besides the band at around 1730 cm^{-1} attributed to C=O stretching (in pristine GNR), new bands appear regarding C–N and C=O stretching of amide bond between PEG moiety and GNR at about 1280 and 1640 cm^{-1}, respectively. In addition, C–O–C stretching of PEG substituent appeared at 1110 cm^{-1} in the FTIR spectra of GNR-PEG and GNR-PEG-FA [41,42]. GNR-PEG and GNR-PEG-FA also exhibited an increased intensity of bands in 2800–3000 cm^{-1} derived from the C–H stretching vibration of PEG chains.

The TGA results for GNR-PEG and GNR-PEG-FA show significant differences with respect to those of GNR-COOH (Fig. S2). In particular, the weight loss of GNR-COOH is 31.8%, while for GNR-PEG and GNR-PEG-FA corresponds to 89.3%, and 81.9% (Table 1), respectively. These weight loss differences are attributed to the thermal decomposition of PEG chains. Thus, considering the residue percentages between 100 and 500 °C, the number of PEG moieties can be calculated in terms of the grafting percentages (GPs). The GNR-PEG and GNR-PEG-FA lead to GPs of 89.4% and 71.7%, respectively (details in the supplementary data). In addition, we could confirm the purification of GNR-PEG and GNR-PEG-FA after thorough dialysis by TGA, analyzing the standard deviation of the weight loss for diverse replicates (Fig. S2, Table 1, details in supplementary data).

After characterizing the PEGylated GNR systems, GNR-PEG and GNR-PEG-FA were non-covalently modified with CPT and then assessed

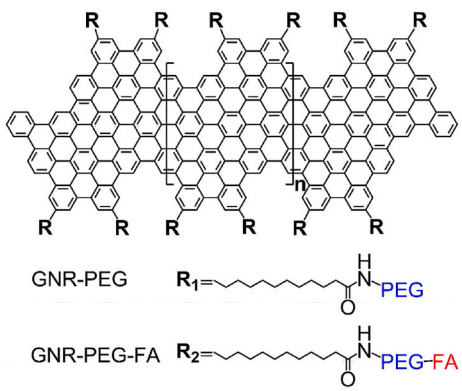

Scheme 1. Structure of GNR derivatives.

Table 1
Quantification of the different functionalities introduced in the GNR systems. [a] obtained from TGA data at 500 °C. [b] This data was calculated by applying *Eq. S1–S2* and *Eq. S3–S4* for GNR-PEG and GNR-PEG-FA, respectively. [c] Obtained from UV–vis absorption spectroscopy data and by applying *Eq. S5* and *S6* for GNR-PEG and GNR-PEG-FA, respectively.

Sample	Weight loss/%[a]	GP/%[b]	LC/%[c]	LE/%[c]
GNR-COOH	31.8 ± 1.5	–	–	–
GNR-PEG	89.3 ± 3.9	89.4 ± 4.2	60.4 ± 4.9	61.0 ± 4.3
GNR-PEG-FA	81.9 ± 3.3	71.7 ± 5.8	71.2 ± 2.0	71.3 ± 2.0

as potential DDs in terms of loading capacity (LC%) and loading efficiency (LE%, *Eq. S5,* and *S6*, respectively). The LC% and LE% of the two PEGylated GNR derivatives were evaluated by UV–vis absorption (see supplementary data). CPT@GNR-PEG displayed a lower LC% and LE% than CPT@GNR-PEG-FA (Table 1). This difference can be attributed to the higher GP of PEG chains for CPT@GNR-PEG-FA, as it increases the hydrophilicity and hinders part of the GNR surface. Thus, we obtain weaker hydrophobicity and lower π-π interactions between GNR and CPT. Notably, the LC% and LE% of these GNR-PEG systems are superior to those of other nanocarriers, such as graphene oxide (GO),[26] liposomes [43,44] and solid lipid nanoparticles [45,46], indicating their potential as DDSs.

The cell anchoring effect of the GNR systems mediated by the FA receptor was evaluated *in vitro*. In particular, A549 (human epithelial, lung, carcinoma) and MCF-7 (human epithelial, breast, adenocarcinoma) were selected because of their low and high level of expression of FA, respectively. We confirmed by flow cytometry immunoassay that our MCF-7 cultures are indeed expressing higher levels of FA receptor, compared to our A549 cultures (Fig. S3). We treated both cell lines with GNR-PEG and GNR-PEG-FA for 24 h, followed by extensive washing and collected bright-field images. In all cases, we observed the presence of material as dark aggregates during the incubation. However, GNR-PEG was totally removed upon extensive washing procedures, whilst aggregates of GNR-PEG-FA were still visibly present, edging both A549 and MCF-7 (Fig. 1), indicating a cell-anchoring effect caused by the presence of FA conjugated to GNR. Then, quantitative analysis (over 650 cells for each line) was performed by selecting all aggregates with a size above 0.4 mm^2, to exclude artifacts related to cellular structures. MCF-7 cells presented the highest number of aggregates (2.5 folds) compared to A549 (0.34 and 0.14 aggregates/cell, respectively). Furthermore, 70% of the selected aggregates in MCF-7 present a size below 5 mm^2 whilst only 37% of the aggregates observed in A549 fall in this size range (Fig. 2). In other words, GNR-PEG-FA accumulates in smaller but more dispersed aggregates over MCF-7, whilst it forms fewer but larger aggregates over A549 (also qualitatively evident in Fig. 1). This is consistent with the higher expression of FA anchoring sites in MCF-7 and indicates that a folic acid-mediated targeting occurs.

We carried out *in vitro* MTT assays to analyze the cytotoxicity of all the compounds (GNR-PEG, GNR-PEG-FA, and the corresponding hybrids loaded with CPT and CPT alone, Fig. 3). Both GNR-PEG and GNR-PEG-FA are not cytotoxic in A549 and MCF-7 (tested up to 250 mg/mL, referred to the material). This is an important feature when planning to use GNR as scaffold for drug delivery. In MCF-7, IC_{50} values of CPT alone, using three different incubation times, are consistently higher (2.5–3 folds) than IC_{50}s of GNR-CPT hybrids, suggesting that the presence of GNR enhances the cytotoxicity of the drug in this cell line. However, CPT@GNR-PEG-FA and CPT@GNR-PEG display comparable activity over cell viability, indicating that the possibility of tagging folic acid receptors is not affecting the activity of the drug, in the experimental conditions employed. Assays performed in A549 showed comparable cytotoxicity between the two CPT@GNR hybrids and CPT alone (Fig. S4).

Finally, we performed preliminary experiments to evaluate the potential of these new hybrids for application in PTT. PTT has emerged as

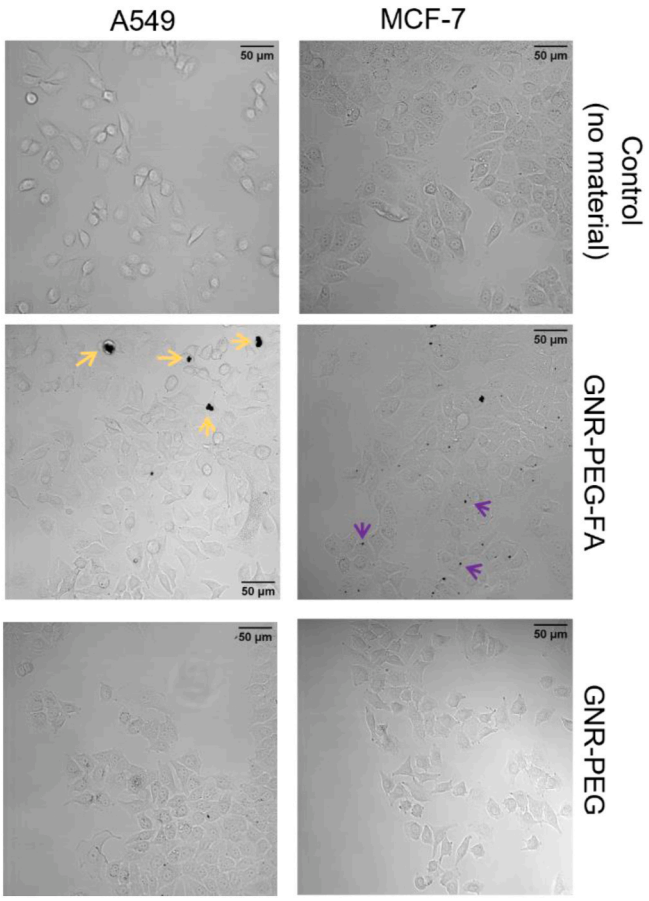

Fig. 1. Bright field images of A549 (left) and MCF-7 (right) incubated with GNR-PEG-FA and GNR-PEG (20 mg/mL) for 24 h, followed by washing and fixation with formalin. Examples of observed GNR-FA aggregates are indicated with yellow (in A549) and magenta (in MCF-7) arrows. Similar aggregates were not observed upon the incubation with GNR (bottom images). (For interpretation of the references to color in this figure legend, the reader is referred to the Web version of this article.)

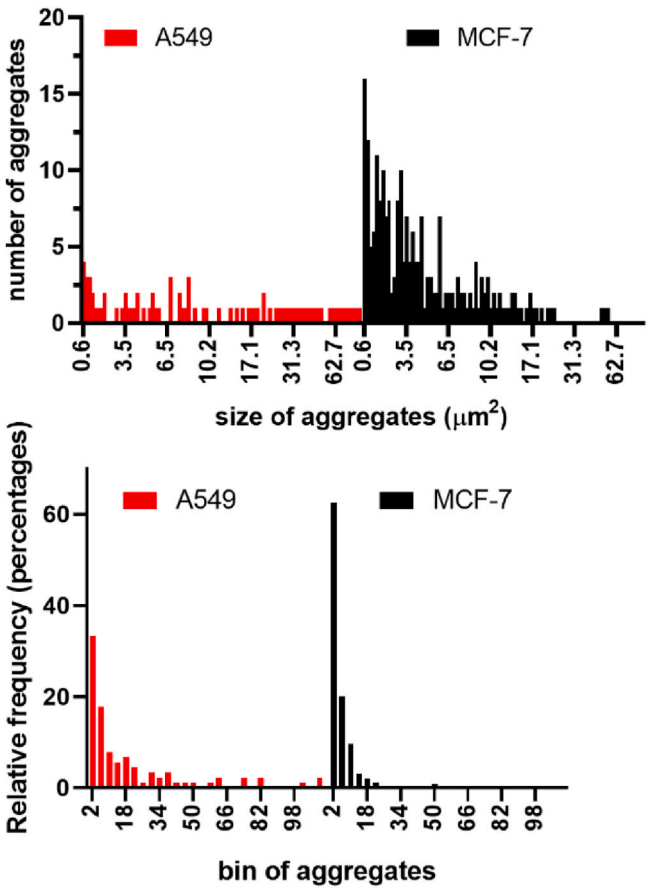

Fig. 2. Quantitative analysis of selected aggregates observed in A549 and MCF-7 upon treatment with GNR-FA (representative examples Fig. 1). Top chart shows the number of aggregates with each measured size (area in mm^2). The frequency distribution, in bottom chart, indicates the relative frequency (%) of each bin of aggregates (bin size 4).

an appealing light-based therapeutic approach for the treatment of diseases in recent years [47,48]. When compared to traditional therapies, the use of light allows for a non-invasive strategy with high specificity. To date, several platforms for PTT have been developed and tested in a variety of disease models [49,50]. For potential use as PTT, graphene GNRs have demonstrated significant photothermal conversion efficiencies. However, *in vivo* applications require targeted biocompatible platforms to limit off-target toxicities and improve therapeutic effects.

First, the absorption spectra of GNR-PEG CPT@ GNR-PEG, GNR-PEG-FA, and CPT@GNR-PEG-FA were evaluated (Fig. S5), exhibiting absorbance across the ultraviolet to NIR range. Importantly, the introduction of CPT loading had minimal impact on the optical properties of the synthesized GNRs within the NIR range. This suggests that these systems are well-suited for applications involving PTT [24,25]. Subsequently, the temperature profiles of materials based on GNRs were examined under an 808 nm laser (Fig. S6). The observed results demonstrated that PEGylated GNR derivatives exhibited rapid and efficient conversion of near-infrared (NIR) laser energy into heat. The maximum temperatures recorded were 51.6 °C, 43.0 °C, 38.6 °C, and 37.2 °C for GNR-PEG, GNR-PEG-FA, CPT@GNR-PEG, and CPT@GNR-PEG-FA, respectively.

Then, *in vitro* studies were performed. We incubated (overnight) A549 cells with GNR-COOH, CPT@GNR-PEG, and CPT alone, followed by a cycle of three irradiation (every 2 h) with a fiber-coupled 808 nm diode laser. At each cycle, cells were exposed to NIR irradiation for 8 min at a monitored temperature of 41 °C (reached during the first minute of irradiation). Cell viability was determined after 2 h from the last cycle of irradiation (Fig. 4). An equivalent set of treated cells was kept in incubator for 18 h, for a comparison with not irradiated cells. First, we could confirm that both GNR-PEG and CPT@GNR-PEG, in this cell culture, are able to heat the sample upon application of NIR light in only 1 min, whilst such heating effect was not observed in the absence of GNRs (cells in their medium only or treated with CPT only). Furthermore, the NIR treatments applied were able to completely affect cell viability, with significantly higher efficiency when compared to cells that were treated with the same compounds but not exposed to irradiation. This result shows the potential of this system for PTT, since complete loss of cell viability was achieved in shorter times (12–18 h), compared to a standard MTT assay, using both the drug loaded and the free material. However, we could not observe relevant differences between the free GNR and any of the hybrids in our hands, at the experimental conditions employed, which include the recommended laser power for this type of application. In other words, the different materials were all efficient for PTT, but not displaying functionalization-depending selectivity, despite different interactions between the materials and cells being clearly observed (Fig. 2). This aspect should be improved, and current studies focus on optimizing the hybrid composition (drug loading, type of functionalization) and the size of the GNR scaffold, to be able to achieve an improved PTT effect at lower concentrations.

In addition, we conducted a dynamic light scattering (DLS) analysis

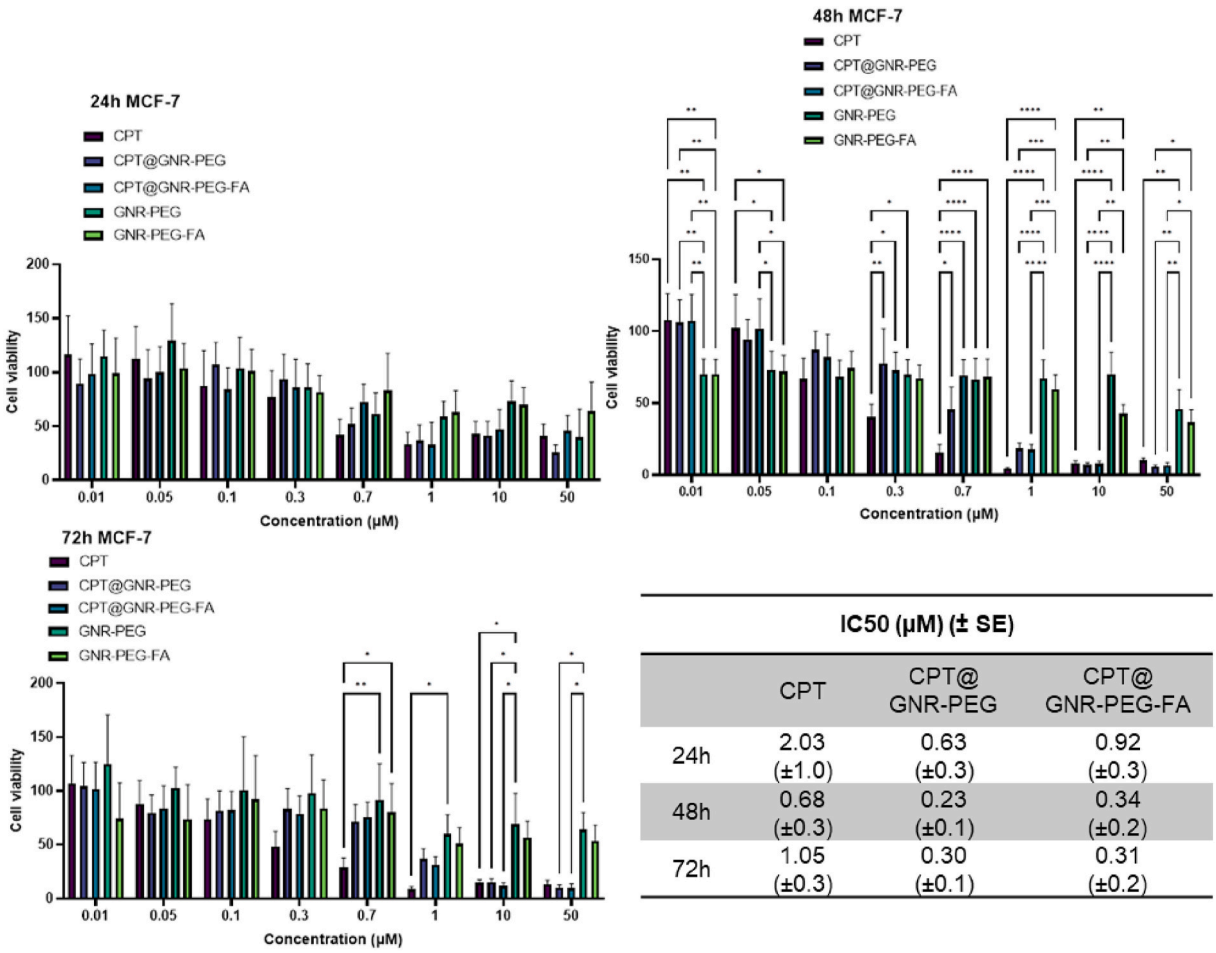

IC50 (μM) (± SE)	CPT	CPT@ GNR-PEG	CPT@ GNR-PEG-FA
24h	2.03 (±1.0)	0.63 (±0.3)	0.92 (±0.3)
48h	0.68 (±0.3)	0.23 (±0.1)	0.34 (±0.2)
72h	1.05 (±0.3)	0.30 (±0.1)	0.31 (±0.2)

Fig. 3. Cell viability by MTT assay of different concentrations of free CPT, GNR-PEG, GNR-PEG -FA, CPT@GNR-PEG, and CPT@GNR-PEG-FA, in MCF-7. 24, 48, and 72 h were used as incubation times. The concentrations reported refer to CPT (in mM) and cell viability is reported as percentage of viable cells in respect to the control (untreated cells). The table (bottom right) reports IC_{50} values for each CPT-containing compound. Each graph was generated with GraphPad Prism 9.1.0 from the average (±SD) of triplicates from at least 2 independent experiments. The multiple comparisons were performed by a two-way ANOVA analysis followed by Tukey's multiple comparison post-hoc test. Significance was graphically indicated as follows: *P *: $P < 0.05$, **: $P < 0.01$, ***: $P < 0.001$.

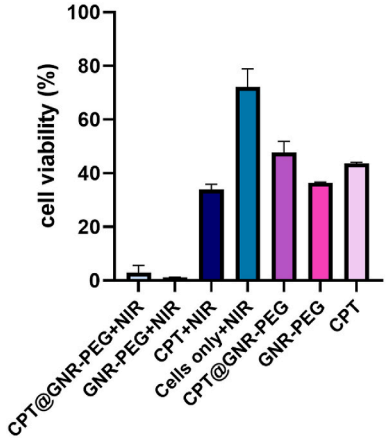

Fig. 4. Cell viability by MTT assay of A549 cells treated with 100 mg/mL of CPT@GNR-PEG, GNR-PEG, and CPT (concentration referred to GNR), upon treatment with NIR (808 nm) and compared with same samples no treated with NIR. Cell viability is reported as percentage of viable cells in respect to the control (cells only, with no material and no NIR irradiation). Data were generated with GraphPad Prism 9.1.0 from the average (±SD) of duplicates from three independent experiments.

for studying possible aggregation processes of GNRs in aqueous solution following laser irradiation (Fig. SX). The analysis revealed similar size distributions for GNR-PEG and CPT@GNR-PEG, with average hydrodynamic diameters (Dh) of 502 and 466 nm, respectively, at a concentration of 0.25 mg/mL in water. Interestingly, a slight reduction in Dh was observed for both materials after irradiation, indicating the absence of aggregation following PTT process.

4. Conclusions

In conclusion, we have synthesized and characterized PEGylated GNR derivatives, GNR-PEG and GNR-PEG-FA, by covalently grafting PEG chains to bottom-up synthesized GNRs. Then, these GNR systems were loaded with CPT by non-covalent interaction to afford CPT@GNR-PEG and CPT@GNR-PEG-FA with excellent LE% and LC%. It is noteworthy It is worth mentioning that while these GNR-based DDSs were specifically modified with the aromatic drug CPT, they possess the capability to accommodate a wide range of drugs, especially those that feature aromatic cores.

The *in vitro* experiments of GNR-PEG and GNR-PEG-FA suggest that functionalization of GNR derivative with folic acid significantly affects their interaction with cells expressing different levels of FA receptor. Both GNR-PEG and GNR-PEG-FA are very much cell compatible, which is a key aspect for applications in drug delivery. Furthermore, these GNR-based materials display remarkable thermal response in standard

cell cultures upon NIR irradiation, causing complete loss of cell viability with few hours of treatment. Although this system shows potential for PTT applications, current efforts focus on achieving systems with improved selectivity. Therefore, we are working on GNR-PEG and GNR-PEG-FA hybrids with different sizes and dispersions, as photothermal responsive scaffolds for different drugs, considering lower levels of drug loading and different types of functionalization (*i.e.*, comparing loading via π-π interaction with functionalization using covalent/cleavable linkers). This research provides new insight into the development of bottom-up synthesized GNRs as DDSs, particularly in conjunction with aromatic core drugs. In addition, it emphasizes the importance of further research on their biocompatibility and as a platform for PTT.

Author contributions

Huilei Hou: conceptualization, investigation, methodology, formal analysis, and writing – original draft. **Lucia Cardo**: investigation, methodology, formal analysis, and writing – review & editing. **Juan Pedro Merino**: investigation and writing – review & editing. **Fugui Xu**: investigation and writing – review & editing. **Cecilia Wetzl**: investigation and writing – review & editing. **Blanca Arnaiz**: investigation and writing – review & editing. **Xiangfeng Luan**: investigation and writing – review & editing. **Yiyong Mai**: conceptualization, methodology, supervision, project administration, funding acquisition, and writing – review & editing. **Alejandro Criado**: conceptualization, methodology, supervision, project administration, funding acquisition, and writing – review & editing. **Maurizio Prato**: conceptualization, methodology, supervision, project administration, funding acquisition, and writing – review & editing.

Declaration of competing interest

The authors declare that they have no known competing financial interests or personal relationships that could have appeared to influence the work reported in this paper.

Data availability

Data will be made available on request.

Acknowledgments

This work was supported by the European Union's Horizon2020 research and innovation program under the Marie Sklodowska-Curie grant (grant no. 734381, CARBO-IMmap). Y. M. and F. X. appreciate the financial support from National Natural Science Foundation of China (52073173, 22225501 and 52203268). H.-L. H. thanks MINECO for his research grant (Juan de la Cierva Incorporacion/no. IJC-2018-037396-I). A. C. acknowledges financial support by Grant RYC2020-030183-I and PID2021-127002NA-I00 funded by MCIN/AEI/10.13039/501100011033 and "ESF Investing in your future". M.P. is the AXA Chair for Bionanotechnology (2016–2026). Part of this work was performed under the Maria de Maeztu Units of Excellence Program from the Spanish State Research Agency, Grant No. MDM-2017- 0720.

References

[1] World Health Organization. Cancer., (n.d.). https://www.who.int/news-room/fact-sheets/detail/cancer.
[2] B.E. Blass, Editorial for cancer virtual issue, ACS Med. Chem. Lett. 8 (2017) 1205–1207, https://doi.org/10.1021/acsmedchemlett.7b00472.
[3] A.G. Waks, E.P. Winer, Breast cancer treatment: a review, J. Am. Med. Assoc. 321 (2019) 288–300, https://doi.org/10.1001/jama.2018.19323.
[4] R. a DePinho, The age of cancer, Nature 408 (2000) 248–254, https://doi.org/10.1038/35041694.
[5] M.B. Sporn, The war on cancer, Lancet 347 (1996) 1377–1381, https://doi.org/10.1016/S0140-6736(96)91015-6.
[6] Z. Zhao, A. Ukidve, J. Kim, S. Mitragotri, Targeting strategies for tissue-specific drug delivery, Cell 181 (2020) 151–167, https://doi.org/10.1016/j.cell.2020.02.001.
[7] K. Cho, X. Wang, S. Nie, Z. Chen, D.M. Shin, Therapeutic nanoparticles for drug delivery in cancer, Clin. Cancer Res. 14 (2008) 1310–1316, https://doi.org/10.1158/1078-0432.CCR-07-1441.
[8] Q. Hu, W. Sun, C. Wang, Z. Gu, Recent advances of cocktail chemotherapy by combination drug delivery systems, Adv. Drug Deliv. Rev. 98 (2016) 19–34, https://doi.org/10.1016/j.addr.2015.10.022.
[9] J.L. Li, B. Tang, B. Yuan, L. Sun, X.G. Wang, A review of optical imaging and therapy using nanosized graphene and graphene oxide, Biomaterials 34 (2013) 9519–9534, https://doi.org/10.1016/j.biomaterials.2013.08.066.
[10] Z. Gu, S. Zhu, L. Yan, F. Zhao, Y. Zhao, Graphene-based smart platforms for combined cancer therapy, Adv. Mater. 31 (2019) 1–27, https://doi.org/10.1002/adma.201800662.
[11] T. Viseu, C.M. Lopes, E. Fernandes, M.E.C.D. Real Oliveira, M. Lúcio, A systematic review and critical analysis of the role of graphene-based nanomaterials in cancer theranostics, Pharmaceutics 10 (2018), https://doi.org/10.3390/pharmaceutics10040282.
[12] A.A. Ghawanmeh, G.A.M. Ali, H. Algarni, S.M. Sarkar, K.F. Chong, Graphene oxide-based hydrogels as a nanocarrier for anticancer drug delivery, Nano Res. 12 (2019) 973–990, https://doi.org/10.1007/s12274-019-2300-4.
[13] D.K. Ji, C. Ménard-Moyon, A. Bianco, Physically-triggered nanosystems based on two-dimensional materials for cancer theranostics, Adv. Drug Deliv. Rev. 138 (2019) 211–232, https://doi.org/10.1016/j.addr.2018.08.010.
[14] H. Zhao, R. Ding, X. Zhao, Y. Li, L. Qu, H. Pei, L. Yildirimer, Z. Wu, W. Zhang, Graphene-based nanomaterials for drug and/or gene delivery, bioimaging, and tissue engineering, Drug Discov. Today 22 (2017) 1302–1317, https://doi.org/10.1016/j.drudis.2017.04.002.
[15] S. Rahimi, Y. Chen, M. Zareian, S. Pandit, I. Mijakovic, Cellular and subcellular interactions of graphene-based materials with cancerous and non-cancerous cells, Adv. Drug Deliv. Rev. 189 (2022), 114467, https://doi.org/10.1016/j.addr.2022.114467.
[16] L. Jiao, L. Zhang, X. Wang, G. Diankov, H. Dai, Narrow graphene nanoribbons from carbon nanotubes, Nature 458 (2009) 877–880, https://doi.org/10.1038/nature07919.
[17] D.V. Kosynkin, A.L. Higginbotham, A. Sinitskii, J.R. Lomeda, A. Dimiev, B.K. Price, J.M. Tour, Longitudinal unzipping of carbon nanotubes to form graphene nanoribbons, Nature 458 (2009) 872–876, https://doi.org/10.1038/nature07872.
[18] L.C. Campos, V.R. Manfrinato, J.D. Sanchez-Yamagishi, J. Kong, P. Jarillo-Herrero, Anisotropic etching and nanoribbon formation in single-layer graphene, Nano Lett. 9 (2009) 2600–2604, https://doi.org/10.1021/nl900811r.
[19] A. Narita, Z. Chen, Q. Chen, K. Müllen, Solution and on-surface synthesis of structurally defined graphene nanoribbons as a new family of semiconductors, Chem. Sci. 10 (2019) 964–975, https://doi.org/10.1039/c8sc03780a.
[20] K.Y. Yoon, G. Dong, Liquid-phase bottom-up synthesis of graphene nanoribbons, Mater. Chem. Front. 4 (2020) 29–45, https://doi.org/10.1039/c9qm00519f.
[21] S.M. Chowdhury, C. Surhland, Z. Sanchez, P. Chaudhary, M.A. Suresh Kumar, S. Lee, L.A. Peña, M. Waring, B. Sitharaman, M. Naidu, Graphene nanoribbons as a drug delivery agent for lucanthone mediated therapy of glioblastoma multiforme, Nanomed. Nanotechnol. Biol. Med. 11 (2015) 109–118, https://doi.org/10.1016/j.nano.2014.08.001.
[22] C. Suhrland, J.P. Truman, L.M. Obeid, B. Sitharaman, Delivery of long chain C16 and C24 ceramide in HeLa cells using oxidized graphene nanoribbons, J. Biomed. Mater. Res. B Appl. Biomater. 108 (2020) 1141–1156, https://doi.org/10.1002/jbm.b.34465.
[23] R.S.K. Houtsma, J. de la Rie, M. Stöhr, Atomically precise graphene nanoribbons: interplay of structural and electronic properties, Chem. Soc. Rev. 50 (2021) 6541–6568, https://doi.org/10.1039/D0CS01541E.
[24] Y. Shang, S. Zhang, H.Q. Gan, K.C. Yan, F. Xu, Y. Mai, D. Chen, X. Le Hu, L. Zou, T. D. James, X.P. He, Targeted photothermal release of antibiotics by a graphene nanoribbon-based supramolecular glycomaterial, Chem. Commun. 59 (2023) 1094–1097, https://doi.org/10.1039/d2cc05879k.
[25] Z.-H. Yu, X. Li, F. Xu, X.-L. Hu, J. Yan, N. Kwon, G.-R. Chen, T. Tang, X. Dong, Y. Mai, D. Chen, J. Yoon, X.-P. He, H. Tian, A supramolecular-based dual-wavelength phototherapeutic agent with broad-spectrum antimicrobial activity against drug-resistant bacteria, Angew. Chem. Int. Ed. 59 (2020) 3658–3664, https://doi.org/10.1002/anie.201913506.
[26] F. Xu, C. Yu, A. Tries, H. Zhang, M. Kläui, K. Basse, M.R. Hansen, N. Bilbao, M. Bonn, H.I. Wang, Y. Mai, Tunable superstructures of dendronized graphene nanoribbons in liquid phase, J. Am. Chem. Soc. 141 (2019) 10972–10977, https://doi.org/10.1021/jacs.9b04927.
[27] X. Luan, C. Martín, P. Zhang, Q. Li, I.A. Vacchi, L.G. Delogu, Y. Mai, A. Bianco, Degradation of structurally defined graphene nanoribbons by myeloperoxidase and the photo-fenton reaction, Angew. Chem. Int. Ed. 59 (2020) 18515–18521, https://doi.org/10.1002/anie.202008925.
[28] Y. Gu, Z. Qiu, K. Müllen, Nanographenes and graphene nanoribbons as multitalents of present and future materials science, J. Am. Chem. Soc. 144 (2022) 11499–11524, https://doi.org/10.1021/jacs.2c02491.

[29] G. Shim, M.-G. Kim, J.Y. Park, Graphene-based nanosheets for delivery of chemotherapeutics and biological drugs, Adv. Drug Deliv. Rev. 105 (2016) 205–227, https://doi.org/10.1016/j.addr.2016.04.004.
[30] C. Greve, L. Jorgensen, V. Agrahari, A.K. Mitra, C. Greve, L. Jorgensen, Therapeutic delivery, Ther. Deliv. 7 (2016) 117–138, https://doi.org/10.4155/tde.15.92.
[31] C. McCallion, J. Burthem, K. Rees-Unwin, A. Golovanov, A. Pluen, Graphene in therapeutics delivery: problems, solutions and future opportunities, Eur. J. Pharm. Biopharm. 104 (2016) 235–250, https://doi.org/10.1016/j.ejpb.2016.04.015.
[32] C. Liao, Y. Li, S.C. Tjong, Graphene nanomaterials: synthesis, biocompatibility, and cytotoxicity, Int. J. Mol. Sci. 19 (2018) 3564, https://doi.org/10.3390/ijms19113564.
[33] E.L. Khim Chng, C.K. Chua, M. Pumera, Graphene oxide nanoribbons exhibit significantly greater toxicity than graphene oxide nanoplatelets, Nanoscale 6 (2014) 10792–10797, https://doi.org/10.1039/c4nr03608e.
[34] O. Akhavan, E. Ghaderi, H. Emamy, Nontoxic concentrations of PEGylated graphene nanoribbons for selective cancer cell imaging and photothermal therapy, J. Mater. Chem. 22 (2012) 20626–20633, https://doi.org/10.1039/c2jm34330d.
[35] Y. Liu, X. Wang, W. Wan, L. Li, Y. Dong, Z. Zhao, J. Qiu, Multifunctional nitrogen-doped graphene nanoribbon aerogels for superior lithium storage and cell culture, Nanoscale 8 (2016) 2159–2167, https://doi.org/10.1039/c5nr05909g.
[36] M. Silva, S.G. Caridade, A.C. Vale, E. Cunha, M.P. Sousa, J.F. Mano, M.C. Paiva, N. M. Alves, Biomedical films of graphene nanoribbons and nanoflakes with natural polymers, RSC Adv. 7 (2017) 27578–27594, https://doi.org/10.1039/c7ra04173j.
[37] S. Mullick Chowdhury, S. Dasgupta, A.E. Mcelroy, B. Sitharaman, Structural disruption increases toxicity of graphene nanoribbons, J. Appl. Toxicol. 34 (2014) 1235–1246, https://doi.org/10.1002/jat.3066.
[38] O. Akhavan, E. Ghaderi, H. Emamy, F. Akhavan, Genotoxicity of graphene nanoribbons in human mesenchymal stem cells, Carbon 54 (2013) 419–431, https://doi.org/10.1016/j.carbon.2012.11.058.
[39] A. Deb, R. Vimala, Camptothecin loaded graphene oxide nanoparticle functionalized with polyethylene glycol and folic acid for anticancer drug delivery, J. Drug Deliv. Sci. Technol. 43 (2018) 333–342, https://doi.org/10.1016/j.jddst.2017.10.025.
[40] L.F. Liu, S.D. Desai, T.K. Li, Y. Mao, M. Sun, S.P. Sim, Mechanism of action of camptothecin, Ann. N. Y. Acad. Sci. 922 (2000) 1–10, https://doi.org/10.1111/j.1749-6632.2000.tb07020.x.
[41] Y. Huang, Y. Mai, U. Beser, J. Teyssandier, G. Velpula, H. Van Gorp, L.A. Straasø, M.R. Hansen, D. Rizzo, C. Casiraghi, R. Yang, G. Zhang, D. Wu, F. Zhang, D. Yan, S. De Feyter, K. Müllen, X. Feng, Poly(ethylene oxide) functionalized graphene nanoribbons with excellent solution processability, J. Am. Chem. Soc. 138 (2016) 10136–10139, https://doi.org/10.1021/jacs.6b07061.
[42] M. de Sousa, L.A. Visani de Luna, L.C. Fonseca, S. Giorgio, O.L. Alves, Folic-acid-functionalized graphene oxide nanocarrier: synthetic approaches, characterization, drug delivery study, and antitumor screening, ACS Appl. Nano Mater. 1 (2018) 922–932, https://doi.org/10.1021/acsanm.7b00324.
[43] Y. Li, R. Liu, J. Yang, G. Ma, Z. Zhang, X. Zhang, Dual sensitive and temporally controlled camptothecin prodrug liposomes codelivery of siRNA for high efficiency tumor therapy, Biomaterials 35 (2014) 9731–9745, https://doi.org/10.1016/j.biomaterials.2014.08.022.
[44] R.D. Whitaker, S.G. Ingebrigtsen, E. Naderkhani, M.L. Skar, G.E. Flaten, Investigation of parameters influencing incorporation, retention and cellular cytotoxicity in liposomal formulations of poorly soluble camptothecin, J. Liposome Res. 23 (2013) 298–310, https://doi.org/10.3109/08982104.2013.805338.
[45] D.J. Jang, C. Moon, E. Oh, Improved tumor targeting and antitumor activity of camptothecin loaded solid lipid nanoparticles by preinjection of blank solid lipid nanoparticles, Biomed. Pharmacother. 80 (2016) 162–172, https://doi.org/10.1016/j.biopha.2016.03.018.
[46] S.M. Martins, B. Sarmento, C. Nunes, M. Lúcio, S. Reis, D.C. Ferreira, Brain targeting effect of camptothecin-loaded solid lipid nanoparticles in rat after intravenous administration, Eur. J. Pharm. Biopharm. 85 (2013) 488–502, https://doi.org/10.1016/j.ejpb.2013.08.011.
[47] J. Seung Lee, J. Kim, Y. sinn Ye, T. il Kim, Materials and device design for advanced phototherapy systems, Adv. Drug Deliv. Rev. 186 (2022), 114339, https://doi.org/10.1016/j.addr.2022.114339.
[48] J. Li, K. Pu, Development of organic semiconducting materials for deep-tissue optical imaging, phototherapy and photoactivation, Chem. Soc. Rev. 48 (2019) 38–71, https://doi.org/10.1039/c8cs00001h.
[49] D. De Melo-Diogo, R. Lima-Sousa, C.G. Alves, I.J. Correia, Graphene family nanomaterials for application in cancer combination photothermal therapy, Biomater. Sci. 7 (2019) 3534–3551, https://doi.org/10.1039/c9bm00577c.
[50] W.T. Dou, F. Xu, C.X. Xu, J. Gao, H.B. Ru, X. Luan, J. Zhang, L. Zhu, A.C. Sedgwick, G.R. Chen, Y. Zang, T.D. James, H. Tian, J. Li, Y. Mai, X.P. He, Graphene nanoribbon-based supramolecular ensembles with dual-receptor targeting function for targeted photothermal tumor therapy, Chem. Sci. 12 (2021) 11089–11097, https://doi.org/10.1039/d1sc02154k.